ACS Photonics

Letter

Cite This: ACS Photonics 2019, 6, 2375−2380

pubs.acs.org/journal/apchd5

Direct Characterization of Carrier Diffusion in Halide-Perovskite Thin Films Using Transient Photoluminescence Imaging

Wenhao Li,[†,‡] Matthew Shao Ran Huang,[†,‡] Srinivas K. Yadavalli,[†] Juan David Lizarazo Ferro,[†,‡] Yuanyuan Zhou,[†] Alexander Zaslavsky,[†,‡] Nitin P. Padture,[†] and Rashid Zia*[,†,‡]

[†]School of Engineering and [‡]Department of Physics, Brown University, 184 Hope Street, Providence, Rhode Island 02912, United States

Supporting Information

ABSTRACT: A high-speed, wide-field photoluminescence (PL) imaging method is established for measuring carrier diffusion in formamidinium lead triiodide ($FAPbI_3$) perovskite thin films. This method allows transient PL imaging with a diffraction limited spatial resolution (~300 nm) and a subnanosecond (500 ps) temporal resolution to directly observe carrier diffusion and reliably estimate diffusivity. Combining this method with background continuous-wave (CW) illumination, carrier diffusivity is found to increase with the background carrier density. This effect is discussed within the context of trap−carrier interactions. Our results suggest that the intrinsic value of carrier diffusivity in the $FAPbI_3$ thin films may be up to a factor of two higher than the value measured in a trap-limited regime under one-sun illumination.

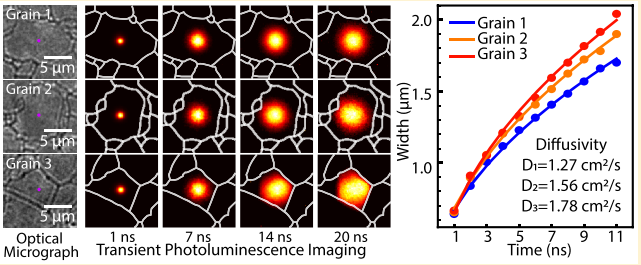

KEYWORDS: *transient photoluminescence imaging, carrier diffusion, carrier recombination, trap screening, perovskite photovoltaic materials*

In recent years, hybrid organic−inorganic halide perovskite solar cells have attracted significant attention due to their high and rapidly increasing power conversion efficiencies. Despite this success achieved through improvements in the fabrication processes and compositional engineering, the underlying optoelectronic properties of these materials, including charge transport, remain controversial. In particular, a better understanding of intrinsic properties could help elucidate the fundamental limits of perovskite thin-film solar cells and help establish guidelines for their further development.

Charge-transport properties are of great relevance to optoelectronic devices, as they determine the quantum efficiency of both photovoltaics and light-emitting diodes. In such devices, the mobility of charge carriers can be limited by both extrinsic and intrinsic factors.[1] Intrinsic factors, such as charge−lattice interactions, cannot be avoided, but extrinsic factors, such as crystal defects and grain boundaries, are qualities that can be engineered to enhance device performance. To study experimentally charge-transport properties, several electrical[2−6] and optical methods[7−21] have been developed to measure carrier diffusivity and mobility.

Optical methods for characterizing carrier diffusivity can be divided into three categories: transient absorption spectroscopy,[12,13] light-induced transient grating spectroscopy,[14−17] and transient photoluminescence (PL) spectroscopy.[18−21] In the former two categories, the changes in light absorption and diffraction efficiency require a high carrier concentration. However, carrier concentration drops quickly with time due to diffusion and recombination, which limits the spatial and temporal window for observing carrier diffusion. Transient PL spectroscopy, on the other hand, can help monitor carrier concentrations over longer time scales. However, conventional time-resolved PL setups with discrete detectors (e.g., avalanche photodiodes or photomultiplier tubes) generally only measure the transient PL at one location on the sample and require repeated measurements at multiple positions to monitor carrier diffusion. The accuracy of such methods can be compromised if the measured locations on the sample are too few; conversely, scanning measurements across the sample may take a long time and may be impacted by sample degradation.

Here, we present a wide-field transient PL imaging method for estimating carrier diffusivity using a fast-gated intensified camera that allows temporal binning with subnanosecond (500 ps) resolution. Compared with conventional transient PL spectroscopy, this method replaces the point detector with a megapixel intensified camera that parallelizes the measurement to achieve diffraction-limited resolution (~300 nm) over a wide observation field (~130 μm). By repeatedly gating the intensifier at fixed-time intervals after the laser excitation pulses, this camera can be used to build up a high signal-to-noise image for a given delay time. The high temporal and spatial resolutions as well as short measurement time allows us to explore carrier diffusion under various conditions. In this paper, we show that this transient PL imaging method can

Received: May 29, 2019
Published: August 26, 2019

DOI: 10.1021/acsphotonics.9b00778
ACS Photonics 2019, 6, 2375−2380

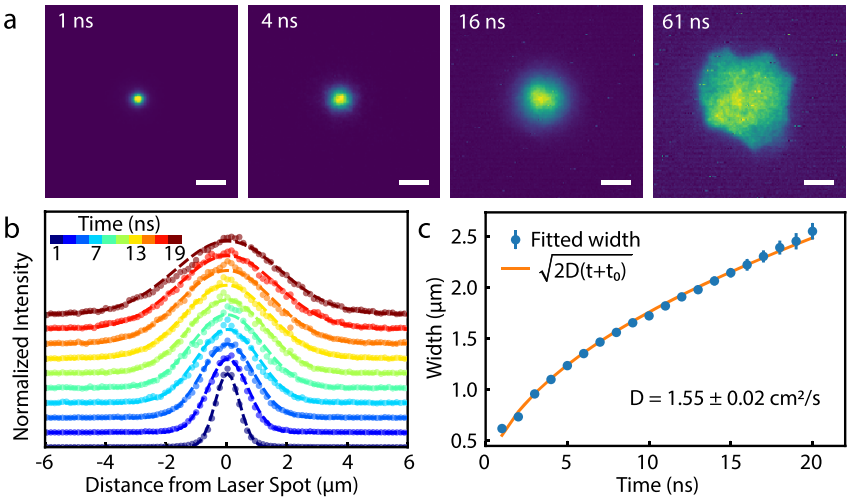

Figure 1. Time-resolved PL imaging measurements of carrier diffusion. (a) Time-resolved PL distribution for 1, 4, 16, and 61 ns time delays after excitation laser pulses. Scale bars are 3 μm. (b) Crosscut of PL distributions and corresponding Gaussian fittings for different time delays. (c) Width of PL distributions fit with a diffusion model, yielding an extracted carrier diffusivity D = 1.55 ± 0.02 cm^2/s.

enable direct characterization of carrier diffusion and, in combination with CW background illumination, can be used to estimate intrinsic limits on carrier mobility.

In particular, we study carrier diffusion in formamidinium lead triiodide ($FAPbI_3$) perovskite thin films. $FAPbI_3$ is a popular perovskite solar cell absorber due to its good thermal stability and desirable bandgap of 1.45 eV. Solar cells with a $FAPbI_3$ absorber with greater than 20% efficiency have been reported.[22] Large-grain (~5 μm) thin films can also be fabricated by using a solvent annealing method.[23] We studied carrier diffusion within individual grains of this material to preclude the confounding effect of grain and subgrain boundaries.[24] Finally, by combining our time-gated measurement technique with CW illumination, we will show that carrier transport in $FAPbI_3$ thin films is in a trap-limited regime, which suggests that this material still has potential for further improvement in power conversion efficiency.

RESULTS AND DISCUSSION

To characterize carrier diffusion, samples were excited by a focused 408 nm pulsed laser. Spatially resolved PL was acquired and imaged onto a fast-gated intensified camera (Princeton Instruments, PI-MAX4). With the help of its picosecond gating function, 1 ns long exposures are repeated for 6.4 × 10^5 cycles at the same delay time with respect to excitation laser pulses (10 kHz repetition rate). The intensifying and binning mechanisms help achieve an improved signal-to-noise ratio while maintaining high temporal and spatial resolution.

The PL images, recorded as a function of time delay with respect to the excitation laser pulses, are shown in Figure 1a. The PL distribution expands with time and keeps an approximate 2D Gaussian shape until it is limited by grain boundaries. Note that this expansion rate cannot be due to light traveling and scattering in the material, because that process would occur at much faster time scales. The slow expansion rate and the barriers observed at grain boundaries indicate that the PL distribution dynamics are related to carrier diffusion in the material. Carriers generated in the illuminated region (near-diffraction-limited, 250 nm spot) diffuse due to the carrier-concentration gradient and ultimately decay through radiative and nonradiative recombination channels. Since the PL intensity $I(x, y, t)$ is proportional to the square of the carrier density $n(x, y, t)$, the PL distribution can be used to infer the dynamics of the carrier density. Note that the exciton binding energy of ~10 meV is small compared to thermal energy,[25] and we observe no excitonic peak in room-temperature absorption spectra. Thus, we assume that primary carriers are free electrons and holes. Given that the diffusion of electrons and holes is linked by their Coulomb attraction, and since their effective masses are close (approximately 3:4 for $FAPbI_3$ and 4:5 for similar $MAPbI_3$ halide perovskite materials[26,27]), we therefore assume that electron and hole diffusivities are not very different. A 2D Gaussian model that describes carrier distribution is used to fit the square root of the PL distribution to extract the Gaussian carrier width $\sigma(t)$, as shown in Figure 1b. Then the $\sigma(t)$ evolution is used to estimate the carrier diffusivity D through[12]

$$\sigma(t) = \sqrt{2D(t + t_0)}$$

where the parameter t_0 is introduced to account for the initial carrier distribution ($|t_0| < 0.1$ ns, see Supporting Information). This diffusion model neglects possible surface diffusion effects, and only holds exactly when linear recombination dominates. The systematic error in estimating diffusivity with this model is discussed in the Supporting Information. The carrier diffusivity in this particular grain is inferred to be 1.55 ± 0.02 cm^2/s.

This method allows us to measure the diffusivity D in each individual grain, which is helpful for understanding the variation of carrier transport within $FAPbI_3$ thin films. Figure 2a shows the corresponding σ evolution for 20 different grains, together with the resulting histogram for diffusivities in Figure 2b (A movie showing transient PL images for the 20 grains is included in the Supporting Information). In each grain, the PL distribution keeps an approximately symmetric 2D Gaussian shape while expanding with time, which indicates that the diffusivity is roughly spatially homogeneous within each grain, even though it varies between 1.3 and 1.8 cm^2/s in the observed grains.

Interestingly, carrier diffusion can be accelerated by applying uniform CW laser illumination to the sample using the configuration shown in Figure 3a, where a homogeneous 401

DOI: 10.1021/acsphotonics.9b00778
ACS Photonics 2019, 6, 2375−2380

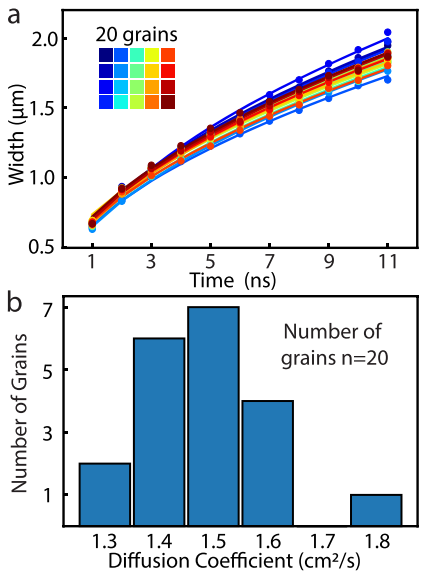

Figure 2. Diffusivity variation in 20 grains. (a) Width evolution of 20 grains and the corresponding fits to the diffusion model. (b) Histogram of diffusivity D for the 20 grains

nm CW laser is applied to the sample, together with the focused pulsed-excitation laser at 408 nm. To observe a large change in carrier diffusivity, a relatively high CW laser power density (150 W/cm^2) is required. Since constant illumination at this power density could heat and decompose the sample, we modulated the CW illumination to be only turned on intermittently for 500 ns when the PL measurement is running, so that the average CW power is sufficiently low at ∼1 W/cm^2 so as not to degrade the sample (a detailed timing diagram can be found in the Supporting Information). Transient PL images were acquired to measure the diffusivity for the carriers generated from the pulsed laser with and without the homogeneous quasi-CW background laser excitation. In order to observe the diffusion of carriers generated by the pulsed laser, the PL distribution under quasi-CW illumination alone was measured and subtracted from the transient PL distribution data.

By fitting the width evolution to the diffusion model, we estimate the diffusivity of the grain in Figure 3 to be 1.2 cm^2/s before the CW illumination, 2.6 cm^2/s under illumination, and returning to 1.3 cm^2/s after illumination, as shown in Figure 3b. Note that the increase in carrier diffusivity induced by the background illumination is reversible, indicating that the increased diffusivity under CW illumination is not due to structural changes in the material.

A possible mechanism for the increase in the diffusivity under background laser illumination is the charge-trap screening effect. In $FAPbI_3$ thin films, traps can capture carriers and limit their mean free path. However, carriers generated by the quasi-CW illumination can fill and neutralize these traps, preventing them from capturing other carriers. Thus, the mean free path of carriers injected by the pulsed laser may be extended by the background illumination, resulting in a higher diffusivity, as is illustrated by the right panel of Figure 3c.

We also performed the previous measurements under quasi-CW laser power densities from 2 to 400 W/cm^2. The 400 W/cm^2 upper bound was chosen because we observed a sharp decrease in PL intensity above 500 W/cm^2 (averaged power density 2.5 W/cm^2); this drop could be due to either the

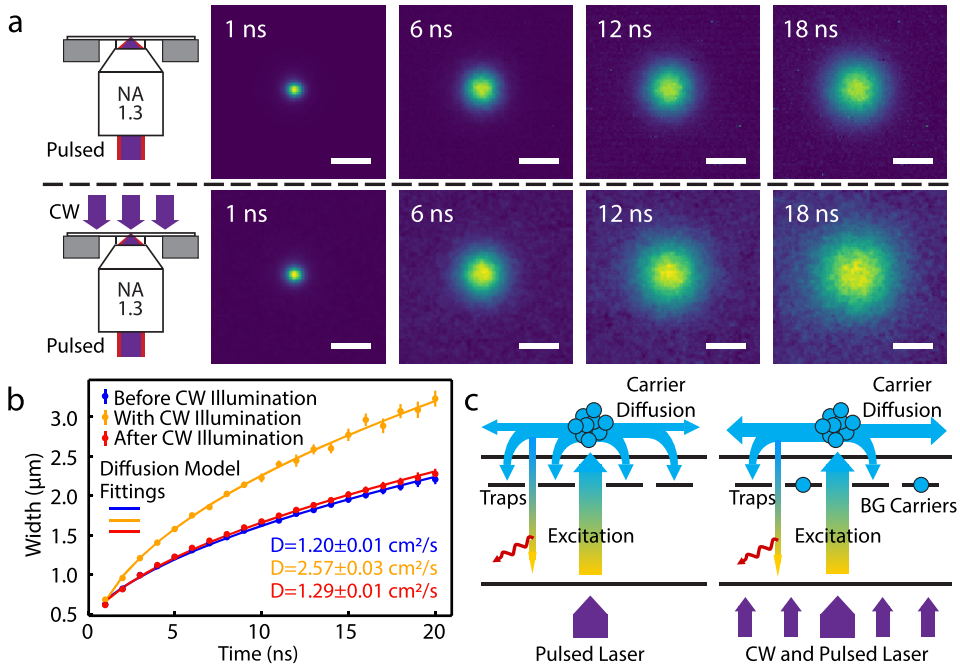

Figure 3. Carrier diffusivity enhancement under quasi-CW uniform laser illumination. (a) Schematic illustration of CW illumination and transient PL distribution evolution under different illumination conditions. Scale bars are 3 μm. (b) Width evolution under different illumination conditions and the corresponding diffusion model fits. The transient PL distribution measurements were taken before applying quasi-CW illumination (blue), with the quasi-CW illumination (yellow), and after turning off the quasi-CW illumination (red). The instantaneous CW illumination power density is 150 W/cm^2, and the average CW illumination power density is 750 mW/cm^2. (c) Schematic illustrating the increase in carrier mean free path by charge trap screening effect.

DOI: 10.1021/acsphotonics.9b00778
ACS Photonics 2019, 6, 2375−2380

increase in sample temperature or heat-related damage. We acquired transient PL images for each power density. Initially, the diffusivity increased with the background laser illumination power, but this effect saturated at a power density of around 250 W/cm^2, as is shown in Figure 4a. Power-dependent carrier

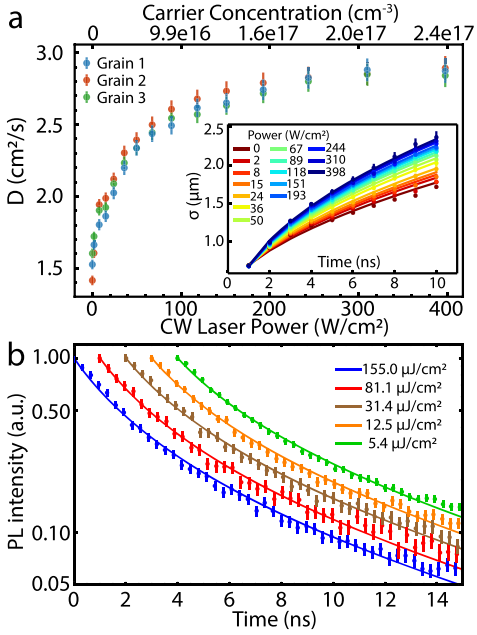

Figure 4. Diffusion and recombination kinetics. (a) Diffusivities of three grains as a function of CW illumination power. Inset shows the PL width evolution under various CW illumination powers for grain 1. (b) Transient PL decay at different pump powers fit with a recombination and diffusion model. The decay curves are shifted consecutively by 1 ns for clarity.

diffusivity measurements were performed on three different grains. Even though the diffusivities for the three grains were different in the dark (1.52 ± 0.03, 1.42 ± 0.03, and 1.60 ± 0.03 cm^2/s for grains 1, 2, and 3, respectively), their saturation values were roughly the same (2.87 ± 0.08, 2.89 ± 0.08, and 2.84 ± 0.08 cm^2/s).

In order to estimate the carrier density under a given background CW laser illumination power, the carrier recombination mechanism needs to be better understood. A transient PL decay experiment was therefore carried out using different pulsed-laser pump energy densities, and the PL signal was measured using a fast single-photon avalanche diode (PicoQuant, τ-SPAD), which has a higher time resolution of 64 ps.

To model the time dynamics of carrier density $n(x, y, t)$, a phenomenological model consisting of Shockley-Read-Hall recombination, bimolecular recombination, and diffusion terms was considered:[28]

$$\frac{\partial n(r,t)}{\partial t} = G + D\nabla^2 n(r,t) - \frac{1}{\tau}n(r,t) - \beta n(r,t)^2 \quad (1)$$

where G corresponds to the carrier generation rate, τ to carrier lifetime, β to bimolecular recombination coefficient, and D to the diffusivity. Given that the film thickness is approximately 450 nm (i.e., negligible given the relevant time scale and diffusivity), the diffusion can be modeled as a 2D process.

Due to the Gaussian shape of the pump beam and the observed rotational symmetry of the PL distributions, the initial carrier density was modeled to be a symmetric Gaussian. By assuming that the PL intensity is proportional to n^2, the numerical solution of this PDE is integrated over the collection area of the optics, and then fit to the normalized time-resolved PL intensity measured by the SPAD. A single set of τ = (3.72 ± 0.05) × 10^{-8} s and β = (2.4 ± 0.2) × 10^{-10} cm^3 s^{-1} values provided a good fit for all five input pump energy densities. Then with the carrier generation rate G calculated from the background illumination power, steady-state carrier concentration can be estimated using eq 1. The corresponding carrier concentration for saturation background illumination power of 250 W/cm^2 is (1.8 ± 0.3) × 10^{17} cm^{-3}.

The measured diffusivity improvement under CW illumination reflects an increase in carrier mean free path, which could result from trap screening by the background carriers. This hypothesis is also consistent with the saturation observed in the power-dependent diffusion measurements shown in Figure 4a. Initially, carrier diffusivity increases with CW laser power as more traps are filled by background carriers; this is a trap-limited regime in which the trap-carrier interactions impede transport. Once the illumination power density reaches ∼250 W/cm^2, carrier diffusivity plateaus as traps become saturated. The trap occupation dynamics can be determined if the trap densities and energy levels are known.[28,29] While the actual trap densities in our samples require further study, our results point to the same order of magnitude as the saturation background carrier concentration (10^{17} cm^{-3}), consistent with previous reports on surface trap density for similar methylammonium lead triiodide ($MAPbI_3$) perovskite material.[30] As shown in Figure 4a, the diffusivity saturation level for multiple grains is quite similar, which suggests that these grains have a similar intrinsic diffusivity and that the difference in their measured diffusivity values in the dark is due to different trap densities. Interestingly, our results suggest that carrier diffusion is still in the trap-limited regime under 1 sun illumination (∼100 mW/cm^2).

In conclusion, we have presented a wide-field transient PL imaging method to measure the carrier diffusivity in perovskite thin films. In contrast to point detectors used in conventional transient PL spectroscopy setups, the fast-gated intensified camera sacrifices picosecond time resolution for parallelized measuring capability that provides diffraction-limited resolution over a wide field of view. In the context of carrier transport studies in organic−inorganic halide perovskites, 1 ns time resolution is sufficient for resolving carrier transport, whereas spatial information over length scales comparable to grain size is important for accurately estimating carrier diffusivity. Using our method, carrier diffusivity changes were studied as a function of background carrier density created by CW illumination and discussed within the context of trap-carrier interactions. We show that, even in the absence of grain and subgrain boundary scattering, the carrier diffusion in $FAPbI_3$ is still in the trap-limited domain under one-sun illumination. Such carrier-trap interactions would impede carrier extraction and ultimately limit the short circuit current and quantum efficiency of solar cell devices.

MATERIALS AND METHODS

Sample Fabrication. The thin films were processed in a N_2-filled glovebox using a method described in ref 23. Briefly, the precursor solution of $FAPbI_3$ was prepared by dissolving FAI (Dyesol, Australia) and PbI_2 (Sigma-Aldrich, U.S.A.) in stoichiometric (1:1) ratio in *N*,*N*-dimethyl formamide (Sigma-

DOI: 10.1021/acsphotonics.9b00778
ACS Photonics 2019, 6, 2375−2380

Aldrich, U.S.A.) to obtain a 45 wt % solution. The solution was spin-coated at 6000 rpm for 45 s onto precleaned glass substrates (Fisher Scientific, 12-548C). At the end of the sixth second during spinning, 300 mL of antisolvent chlorobenzene (Sigma-Aldrich, U.S.A.) was dripped quickly at the center of the film. The thin films were annealed at 95 °C, while being exposed to solvent vapor, for 20 min using a setup similar to that used by Xiao et al.[31] Briefly, the substrate with the as-deposited thin film was placed on a preheated hot plate, then a 10 mL drop of dimethyl sulfoxide (DMSO) was placed 2 cm from the closest edge of the substrate on a glass slide. The substrate and the glass slide with DMSO were covered immediately with an inverted glass Petri dish.

Photoluminescence Measurement. During the optical measurement, the $FAPbI_3$ thin films were kept in nitrogen to reduce the damage from humidity and oxygen. Samples were excited with a 408 nm pulsed laser (PicoQuant, PDL800) focused by an oil immersion objective (Nikon, 100× 1.3 NA). Spatially resolved photoluminescence was collected with the same objective and imaged with a fast-gated intensified camera (Princeton Instruments, PI-MAX4). When acquiring the time-resolved PL data, 1 ns exposures were repeated at a same delay time for 6.4×10^5 cycles to achieve a desirable signal-to-noise ratio. In the power-dependent carrier diffusion experiment, a 401 nm CW laser (Coherent CUBE) was used for illuminating the sample from the top to create background carriers.

■ ASSOCIATED CONTENT

Supporting Information

The Supporting Information is available free of charge on the ACS Publications website at DOI: 10.1021/acsphotonics.9b00778.

Timing diagram for the transient PL distribution measurements; an estimation of the systematic error of carrier diffusivity; and details on fitting the time-resolved PL data with the diffusion-recombination model (PDF)

A movie that shows the time dynamics of the PL distribution (AVI)

■ AUTHOR INFORMATION

Corresponding Author

*E-mail: rashid_zia@brown.edu.

ORCID

Wenhao Li: 0000-0003-2715-0511

Matthew Shao Ran Huang: 0000-0002-7599-1393

Juan David Lizarazo Ferro: 0000-0002-6171-415X

Nitin P. Padture: 0000-0001-6622-8559

Rashid Zia: 0000-0002-2742-5186

Notes

The authors declare no competing financial interest.

■ ACKNOWLEDGMENTS

Funding was provided by the National Science Foundation (OIA-1538893) and the Office of Naval Research (N00014-17-1-2232).

■ REFERENCES

(1) Herz, L. M. Charge-Carrier Mobilities in Metal Halide Perovskites: Fundamental Mechanisms and Limits. *ACS Energy Letters* **2017**, *2*, 1539−1548.

(2) Shi, D.; Adinolfi, V.; Comin, R.; Yuan, M.; Alarousu, E.; Buin, A.; Chen, Y.; Hoogland, S.; Rothenberger, A.; Katsiev, K.; Losovyj, Y.; Zhang, X.; Dowben, P. A.; Mohammed, O. F.; Sargent, E. H.; Bakr, O. M. Low Trap-state Density and Long Carrier Diffusion in Organolead Trihalide Perovskite Single Crystals. *Science* **2015**, *347*, 519−522.

(3) Dong, Q.; Fang, Y.; Shao, Y.; Mulligan, P.; Qiu, J.; Cao, L.; Huang, J. Electron-hole Diffusion Lengths > 175 μm in Solution-grown $CH_3NH_3PbI_3$ Single Crystals. *Science* **2015**, *347*, 967−970.

(4) Saidaminov, M. I.; Abdelhady, A. L.; Murali, B.; Alarousu, E.; Burlakov, V. M.; Peng, W.; Dursun, I.; Wang, L.; He, Y.; Maculan, G.; Goriely, A.; Wu, T.; Mohammed, O. F.; Bakr, O. M. High-quality Bulk Hybrid Perovskite Single Crystals within Minutes by Inverse Temperature Crystallization. *Nat. Commun.* **2015**, *6*, 7586.

(5) Zhumekenov, A. A.; Saidaminov, M. I.; Haque, M. A.; Alarousu, E.; Sarmah, S. P.; Murali, B.; Dursun, I.; Miao, X.-H.; Abdelhady, A. L.; Wu, T.; Mohammed, O. F.; Bakr, O. M. Formamidinium Lead Halide Perovskite Crystals with Unprecedented Long Carrier Dynamics and Diffusion Length. *ACS Energy Letters* **2016**, *1*, 32−37.

(6) Maculan, G.; Sheikh, A. D.; Abdelhady, A. L.; Saidaminov, M. I.; Haque, M. A.; Murali, B.; Alarousu, E.; Mohammed, O. F.; Wu, T.; Bakr, O. M. $CH_3NH_3PbCl_3$ Single Crystals: Inverse Temperature Crystallization and Visible-Blind UV-Photodetector. *J. Phys. Chem. Lett.* **2015**, *6*, 3781−3786.

(7) Wehrenfennig, C.; Eperon, G. E.; Johnston, M. B.; Snaith, H. J.; Herz, L. M. High Charge Carrier Mobilities and Lifetimes in Organolead Trihalide Perovskites. *Adv. Mater.* **2014**, *26*, 1584−1589.

(8) Eperon, G. E.; Leijtens, T.; Bush, K. A.; Prasanna, R.; Green, T.; Wang, J. T.-W.; McMeekin, D. P.; Volonakis, G.; Milot, R. L.; May, R.; Palmstrom, A.; Slotcavage, D. J.; Belisle, R. A.; Patel, J. B.; Parrott, E. S.; Sutton, R. J.; Ma, W.; Moghadam, F.; Conings, B.; Babayigit, A.; Boyen, H.-G.; Bent, S.; Giustino, F.; Herz, L. M.; Johnston, M. B.; McGehee, M. D.; Snaith, H. J. Perovskite-perovskite Tandem Photovoltaics with Optimized Band Gaps. *Science* **2016**, *354*, 861−865.

(9) Milot, R. L.; Eperon, G. E.; Snaith, H. J.; Johnston, M. B.; Herz, L. M. Temperature Dependent Charge-Carrier Dynamics in $CH_3NH_3PbI_3$ Perovskite Thin Films. *Adv. Funct. Mater.* **2015**, *25*, 6218−6227.

(10) Ponseca, C. S.; Savenije, T. J.; Abdellah, M.; Zheng, K.; Yartsev, A.; Pascher, T.; Harlang, T.; Chabera, P.; Pullerits, T.; Stepanov, A.; Wolf, J.-P.; Sundström, V. Organometal Halide Perovskite Solar Cell Materials Rationalized: Ultrafast Charge Generation, High and Microsecond-Long Balanced Mobilities, and Slow Recombination. *J. Am. Chem. Soc.* **2014**, *136*, 5189−5192.

(11) Rehman, W.; Milot, R. L.; Eperon, G. E.; Wehrenfennig, C.; Boland, J. L.; Snaith, H. J.; Johnston, M. B.; Herz, L. M. Charge-Carrier Dynamics and Mobilities in Formamidinium Lead Mixed-Halide Perovskites. *Adv. Mater.* **2015**, *27*, 7938−7944.

(12) Guo, Z.; Manser, J. S.; Wan, Y.; Kamat, P. V.; Huang, L. Spatial and Temporal Imaging of Long-range Charge Transport in Perovskite Thin Films by Ultrafast Microscopy. *Nat. Commun.* **2015**, *6*, 7471.

(13) Hill, A. H.; Smyser, K. E.; Kennedy, C. L.; Massaro, E. S.; Grumstrup, E. M. Screened Charge Carrier Transport in Methylammonium Lead Iodide Perovskite Thin Films. *J. Phys. Chem. Lett.* **2017**, *8*, 948−953.

(14) Ščajev, P.; Aleksiejunas, R.; Miasojedovas, S.; Nargelas, S.; Inoue, M.; Qin, C.; Matsushima, T.; Adachi, C.; Jursenas, S. Two Regimes of Carrier Diffusion in Vapor Deposited Lead-Halide Perovskites. *J. Phys. Chem. C* **2017**, *121*, 21600−21609.

(15) Ščajev, P.; Qin, C.; Aleksiejunas, R.; Baronas, P.; Miasojedovas, S.; Fujihara, T.; Matsushima, T.; Adachi, C.; Jursenas, S. Diffusion Enhancement in Highly Excited $MAPbI_3$ Perovskite Layers with Additives. *J. Phys. Chem. Lett.* **2018**, *9*, 3167−3172.

(16) Arias, D. H.; Moore, D. T.; van de Lagemaat, J.; Johnson, J. C. Direct Measurements of Carrier Transport in Polycrystalline Methylammonium Lead Iodide Perovskite Films with Transient Grating Spectroscopy. *J. Phys. Chem. Lett.* **2018**, *9*, 5710−5717.

(17) Guo, Z.; Zhou, N.; Williams, O. F.; Hu, J.; You, W.; Moran, A. M. Imaging Carrier Diffusion in Perovskites with a Diffractive Optic-

DOI: 10.1021/acsphotonics.9b00778
ACS Photonics 2019, 6, 2375−2380

Based Transient Absorption Microscope. *J. Phys. Chem. C* **2018**, *122*, 10650−10656.
(18) Tian, W.; Zhao, C.; Leng, J.; Cui, R.; Jin, S. Visualizing Carrier Diffusion in Individual Single-Crystal Organolead Halide Perovskite Nanowires and Nanoplates. *J. Am. Chem. Soc.* **2015**, *137*, 12458−12461.
(19) Tian, W.; Leng, J.; Zhao, C.; Jin, S. Long-Distance Charge Carrier Funneling in Perovskite Nanowires Enabled by Built-in Halide Gradient. *J. Am. Chem. Soc.* **2017**, *139*, 579−582.
(20) Ciesielski, R.; Schafer, F.; Hartmann, N. F.; Giesbrecht, N.; Bein, T.; Docampo, P.; Hartschuh, A. Grain Boundaries Act as Solid Walls for Charge Carrier Diffusion in Large Crystal MAPI Thin Films. *ACS Appl. Mater. Interfaces* **2018**, *10*, 7974−7981.
(21) Karimata, I.; Ohta, K.; Kobori, Y.; Tachikawa, T. Several Orders of Magnitude Difference in Charge-Transfer Kinetics Induced by Localized Trapped Charges on Mixed Halide Perovskites. *ACS Appl. Mater. Interfaces* **2018**, *10*, 37057−37066.
(22) Yang, W. S.; Noh, J. H.; Jeon, N. J.; Kim, Y. C.; Ryu, S.; Seo, J.; Seok, S. I. High performance Photovoltaic Perovskite Layers Fabricated through Intramolecular Exchange. *Science* **2015**, *348*, 1234−1237.
(23) Yadavalli, S. K.; Zhou, Y.; Padture, N. P. Exceptional Grain Growth in Formamidinium Lead Iodide Perovskite Thin Films Induced by the δ-to-α Phase Transformation. *ACS Energy Lett.* **2018**, *3*, 63−64.
(24) Li, W.; Yadavalli, S. K.; Lizarazo-Ferro, D.; Chen, M.; Zhou, Y.; Padture, N. P.; Zia, R. Subgrain Special Boundaries in Halide Perovskite Thin Films Restrict Carrier Diffusion. *ACS Energy Letters* **2018**, *3*, 2669−2670.
(25) Galkowski, K.; Mitioglu, A.; Miyata, A.; Plochocka, P.; Portugall, O.; Eperon, G. E.; Wang, J. T.-W.; Stergiopoulos, T.; Stranks, S. D.; Snaith, H. J.; Nicholas, R. J. Determination of The Exciton Binding Energy and Effective Masses for Methylammonium and Formamidinium Lead Tri-halide Perovskite Semiconductors. *Energy Environ. Sci.* **2016**, *9*, 962−970.
(26) Wang, J.-F.; Fu, X.-N.; Wang, J.-T. First-principles Analysis of The Structural, Electronic, and Elastic Properties of Cubic Organic−inorganic Perovskite $HC(NH_2)_2PbI_3$. *Chin. Phys. B* **2017**, *26*, 106301.
(27) Giorgi, G.; Fujisawa, J.-I.; Segawa, H.; Yamashita, K. Small Photocarrier Effective Masses Featuring Ambipolar Transport in Methylammonium Lead Iodide Perovskite: A Density Functional Analysis. *J. Phys. Chem. Lett.* **2013**, *4*, 4213−4216.
(28) Shockley, W.; Read, W. T. Statistics of the Recombinations of Holes and Electrons. *Phys. Rev.* **1952**, *87*, 835−842.
(29) Simmons, J.; Taylor, G. Nonequilibrium Steady-State Statistics and Associated Effects for Insulators and Semiconductors Containing an Arbitrary Distribution of Traps. *Phys. Rev. B* **1971**, *4*, 502−511.
(30) Xing, G.; Mathews, N.; Lim, S. S.; Yantara, N.; Liu, D.; Sabba, X.; Gratzel, M.; Mhaisalkar, S.; Sum, T. C. Low-temperature Solution-processed Wavelength-tunable Perovskites for Lasing. *Nat. Mater.* **2014**, *13*, 476−480.
(31) Xiao, Z.; Dong, Q.; Bi, C.; Shao, Y.; Yuan, Y.; Huang, J. Solvent Annealing of Perovskite Induced Crystal Growth for Photovoltaic Device Efficiency Enhancement. *Adv. Mater.* **2014**, *26*, 6503−6509.

DOI: 10.1021/acsphotonics.9b00778
ACS Photonics 2019, 6, 2375−2380